Supplementary Materials

Superior energy-storage performance in 0.85Bi$_{0.5}$Na$_{0.5}$TiO$_3$-0.15NaNbO$_3$ lead-free ferroelectric ceramics via composition and microstructure engineering

Chao Zhang,[‡][a] Wenrong Xiao,[‡][a] Fangfang Zeng,[a] Dong Su,[a] Kang Du,[a] Shiyong Qiu,[a] Haibo Zhang,[b] Shenglin Jiang,[a,c] Jia-Min Wu*[b], Guangzu Zhang*[a],

[a]*School of Optical and Electronic Information, Engineering Research Center for Functional Ceramics MOE and Wuhan National Laboratory for Optoelectronics, Huazhong University of Science and Technology, Wuhan 430074, China.*

[b]*State Key Laboratory of Materials Processing and Die & Mould Technology, School of Materials Science and Engineering, Huazhong University of Science and Technology, Wuhan 430074, China*

[c]*Shenzhen Huazhong University of Science and Technology Research Institute, Shenzhen, 518057, China*

‡ Chao Zhang and Wenrong Xiao contributed equally to this work

*Corresponding authors. E-mail addresses: jiaminwu@hust.edu.cn (Jia-Min Wu); zhanggz@hust.edu.cn (Guangzu Zhang).

Experimental section

Sample preparation

The lead-free $(1-x)(0.85Bi_{0.5}Na_{0.5}TiO_3-0.15NaNbO_3)-x(Sr_{1.05}Bi_{0.3})ScO_3$ ceramics were fabricated by a solid-state reaction method using $BaCO_3$ (99.7% purity), TiO_2 (98% purity), Na_2CO_3 (99.8% purity), Nb_2O_5 (99.5% purity), $SrCO_3$ (99.53% purity) and Sc_2O_3 (99.9% purity) powders as raw materials. After ball-milling, the powder mixtures were calcined at 850 ℃ and ball milled again. The calcined powders were mixed with a polyvinyl alcohol solution (PVA) as the binder, and then uniaxially pressed into disks (~0.15 cm in thickness and ~1.2 cm in diameter). Thereafter, the pre-pressed pellets were compacted again with a cold isostatic pressing process. To provide the Bi and Na atmosphere during the sintering process, we choose the deactivated ceramic powder as the landfill material, which has the same chemical composition as the matrix material, and cover it on the raw ceramic pellets before sintering. After being sintered at 1150 ℃-1250 ℃ for 2 h, the obtained ceramics were polished and sputtered with gold electrodes for the electrical measurement.

Sample characterization

The micromorphology and element distribution of the samples were characterized by a field emission scanning electron microscopy (FE-SEM) (Zeiss Geminisem 300). To observe the phase structure and composition of the ceramics, X-ray diffraction (XRD) (7000S/L, Shimadzu Corp., Japan) system was employed. To further confirm the crystal structure, a field emission transmission electron microscopy (FTEM) (Tecnai G2 F30) was employed to get the high-resolution electron microscopy (HREM), and energy dispersive spectroscopy (EDS). The

temperature-dependent dielectric characteristics were performed using a dielectric properties test system (DPTS-AT-600, Wuhan Yanhe Technology Co., Ltd). The polarization-electric field hysteresis loops (*P-E* loops) under different temperature and frequency were recorded by a ferroelectric test system (PolyK Technologies, USA). In the process of testing the temperature stability and frequency stability of ceramics, the external temperature and frequency change sharply. When high voltage is applied on the bulk ceramic, it is easy to accumulate stress and heat in the bulk material, and then lead to the breakdown, which is unfavorable for testing the energy storage performance of materials in a wide temperature and frequency range. Thus, relatively low electric field (300 kV/cm) was applied on the bulk ceramic for the testing of temperature and frequency stability. The breakdown strength of bulk ceramics (~100 μm in thickness) was tested by a high-field breakdown testing system (PolyK Technologies, USA), and the breakdown strength of the specimens was calculated by the Weibull statistics. The energy charging-discharging performance was collected by a charge-discharge measurement system (PK-CPR1701, PolyK Technologies, PA, USA).
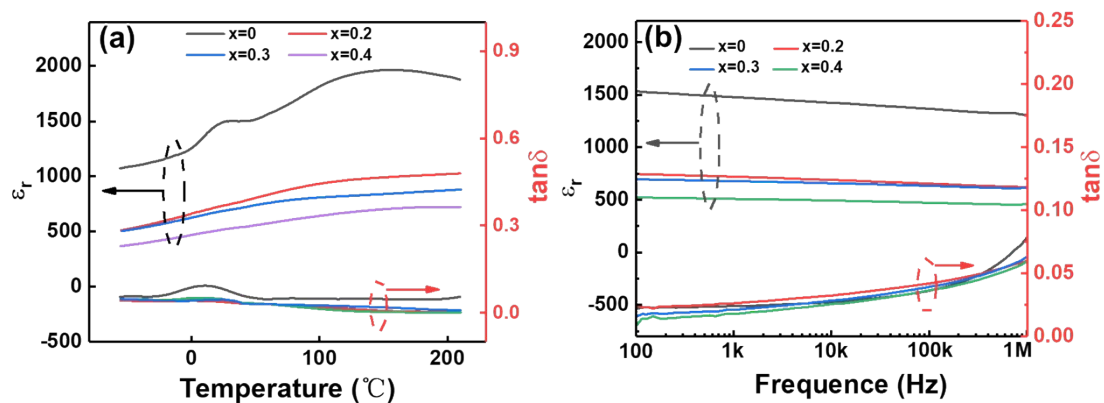

Fig. S1 (a)The temperature dependence of dielectric permittivity (ε_r) and dielectric loss (*tan δ*) of the (1-x)(BNT-NN)-xSBS (x=0.0 , 0.2, 0.3 and 0.4) under 1 kHz. (b) The plot of ε_r and *tan δ* as function of frequencies for (1-x)(BNT-NN)-xSBS ceramics.
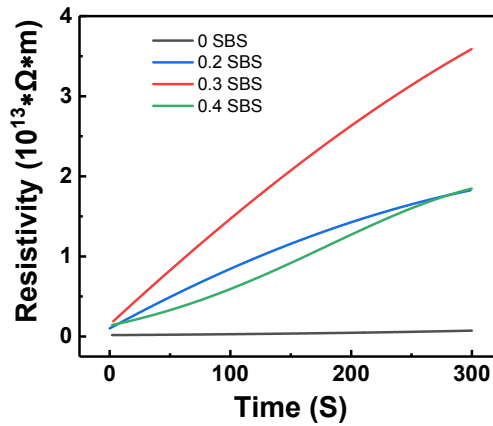
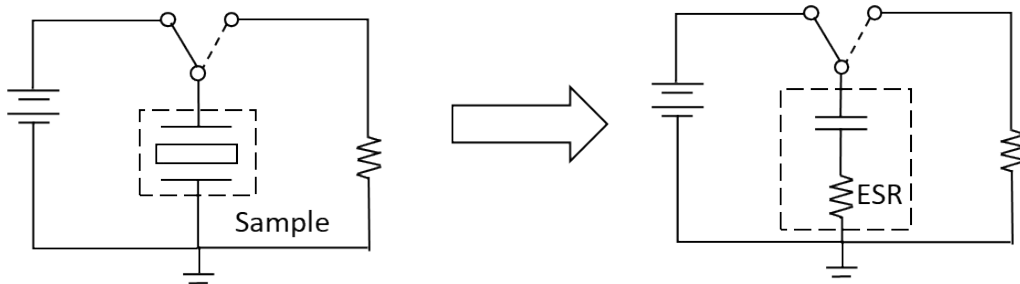Fig. S2 Resistivity of the samples with different content of SBS.

Fig. S3 Schematic diagram of the fast discharge experiment circuit.

In the actual application environment, the discharged energy density (W_{dis}) and discharged time ($t_{0.9}$) can be obtained through charge-discharge measurements using a specific circuit shown in the Fig. S3 above [*Prog. Mater. Sci.* 2019, 102, 72]. The capacitor is first charged by external bias, and then, through a high-speed and high-voltage switch, the total stored energy (W_{tol}) is partly discharged to a load resistor (R_L). According to the formula ($W_{dis}=W_{tol}(R_L+ESR)/R_L$), we can learn that the W_{dis} is highly related to the value of R_L and the equivalent resistor of sample (ESR). It is easy to see that when the external load resistor R_L is much larger than ESR, most of the stored energy will be delivered to the load and thus measured energy density in the discharge method will be nearly the same as the total energy density. However, studies have shown that high external load

resistance will greatly reduce the discharge speed [*IEEE T. Dielect. El. In.* 2006, 13, 1162]. Therefore, compared with 1 kΩ and 100 KΩ resistance equipped in our test circuit，selecting the external load with compromise resistance (13 kΩ) can make the measurement of W_{dis} and $t_{0.9}$ more objective.